ISSN 1330-3651 (Print), ISSN 1848-6339 (Online) https://doi.org/10.17559/TV-20230621000754
Original scientific paper

Load-Displacement Characteristics for Out-of-Plane of Unreinforced Masonry Walls

Liu SHI*, Jingyuan GUO, Songlin ZHAO, Jianguo LIANG, Guanxing CHEN

Abstract: Seismic damage shows that the out-of-plane collapse of unreinforced masonry walls is very common. Especially in the teaching buildings, the out-of-plane collapse of the longitudinal load-bearing walls leads to the disproportionate collapse of the building, which results in serious loss of life and property. It is assumed that the in-plane stiffness of the unreinforced masonry floor system is infinite, and the effect of the integral bending of building on the story drift is ignored. The load-displacement relationship for out-of-plane of unreinforced wall under vertical dead load and horizontal seismic load was deduced with the bilinear constitutive relationship of masonry under compression, the second-order effect of vertical load on deformation being considered. The influence of axial compression ratio and the height-thickness ratio of the wall on the failure model and the load-displacement characteristics in the elastic state, ultimate state and collapse state were also studied. A theoretical method for the collapse mechanism and the aseismic design of the unreinforced masonry structure based on displacement was provided. This study has significant implications for the seismic performance design, post earthquake structural reinforcement, and seismic grade evaluation of unreinforced masonry structures.

Keywords: disproportionate collapse; P-Δ curve; out-of-plane; second-order effect; seismic design; unreinforced masonry

1 INTRODUCTION

Earthquake damage shows that unreinforced masonry buildings without anti-seismic design are damaged or collapsed seriously [1]. There are many such houses in existing Chinese buildings, including rural houses in remote areas, masonry structures built before the promulgation of the seismic design code, and historical protection buildings. The strength/mass ratio of unreinforced masonry structure is quite small frequently, and the inertial force is not constrained in the direction outside the plane, which is prone to the occurrence of brittle failure outside the plane and the formation of brittle collapse mechanism [2].

In order to evaluate the out-of-plane seismic performance of the walls of unreinforced masonry buildings, domestic and foreign scholars have studied the collapse process and collapse mechanism of unreinforced masonry structures by using shaking table test, pseudo-dynamic test and computer simulation [3-9]. These studies are related to the load - displacement characteristics of unreinforced masonry walls. At present, there are mainly two types of rigid body model. One is the rigid body model, which compares the wall cracking under the action of external load to the rigid body movement, and establishes bilinear P-Δ model for structural dynamics analysis [10-14]. The second is the semi-rigid model. The wall is assumed as an elastic-plastic compression member, and the influence of second-order deformation on the stability of the structure is considered. When the maximum compressive strain of the section exceeds the ultimate compressive strain, the member moves according to the rigid body. In these studies, the influence of vertical load eccentricity, different supporting conditions at both ends of the wall, construction quality [15-18] and other factors were considered respectively. In addition, static test, dynamic test, field test, or existing constitutive relation [19-24] are adopted to study the mechanism of wall collapse outside the plane by using the established trilinear P-Δ model.

The above studies are based on non-load-bearing walls. Vertical load only considers the structural dead weight, while horizontal load is the inertial force generated by the wall's dead weight, which is evenly distributed along the wall height without considering the influence of the displacement between floors. However, in the Wenchuan earthquake and Yushu earthquake, many mixed-structure teaching buildings with vertical and horizontal walls and load-bearing structures of primary and secondary schools collapsed [1]. This kind of house in the big earthquake, the horizontal load bearing the transverse wall cracking, resulting in the horizontal displacement of the floor greatly increased, and the floor load of the deep beam to the window wall compressive stress. The displacement of the collapse outside the plane is very small, and the wall between the longitudinal load-bearing windows is easy to collapse outside the plane, leading to the whole collapse of the building.

There is very little theoretical research and experimental research on unreinforced masonry out of plane, and the data is incomplete, which cannot guide the design and seismic performance analysis of unreinforced masonry out of plane. It is not possible to evaluate the seismic performance of each wall in the masonry structure. This article adopts the interlayer shear model. Under the action of vertical loads and horizontal displacements transmitted from the floor, utilizing the existing masonry constitutive relationship and considering material nonlinearity, a semi rigid model method is adopted, derived the P formula for the entire process of unreinforced masonry wall panels bearing horizontal displacement out of plane from loading to collapse - Δ Load displacement relationship. The relationship between the load displacement curve of the wall at different stages and the vertical load and the wall height thickness ratio is studied. It provides a theoretical basis for analyzing and studying the collapse mechanism of masonry walls under earthquake and seismic evaluation and reinforcement of existing unreinforced masonry buildings.

2 ANALYSIS MODEL

In the multi-story rigid scheme, the non-reinforced masonry houses have large stiffness and few layers. Under the horizontal earthquake, shear deformation is the main deformation, and the floor does not rotate. The masonry walls can be regarded as the bearing members with fixed ends at the bottom and moving fixed supports at the top. The calculation diagram is shown in Fig. 1.

Under seismic action, the vertical load N at the top of the wall is assumed to be constant. Under the action of horizontal earthquake, the horizontal displacement between floors is Δ, and the wall top bears the concentrated out-of-plane load P. It is worth noting that the dead weight will also cause the inertia force along the wall height in the earthquake, but the effect on the load-bearing wall, relative to the horizontal displacement of the wall top, can be ignored.

Obviously, the horizontal displacement between floors caused by earthquake will increase the eccentricity of the longitudinal wall, reduce the compressive bearing capacity and stability of the wall, and promote the failure and collapse of the bearing longitudinal wall. In order to analyze the relationship between load and displacement during the failure and collapse of load-bearing walls, the following assumptions are made.

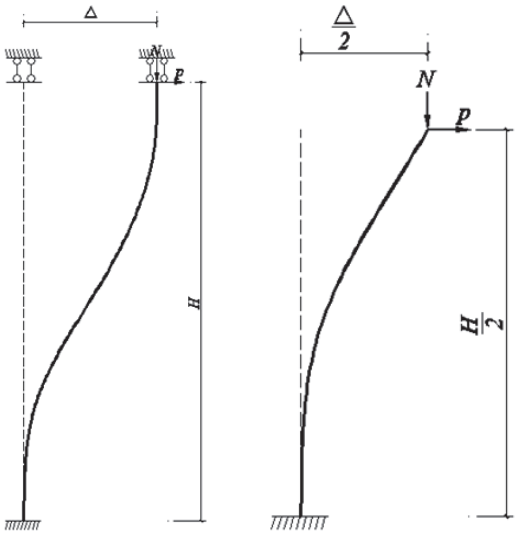

Figure 1 Wall calculation diagram

(1) The stress and strain curve of masonry under compression is shown in Fig. 2, which is an ideal elastic-plastic material. The elastic modulus is E, the compressive strength is f_m, the peak compressive strain is $\varepsilon_p = 0.002$, and the ultimate compressive strain is $\varepsilon_u = 0.0035$.

(2) The section strain conforms to the condition of plane section;

(3) Ignoring the tensile strength of masonry.

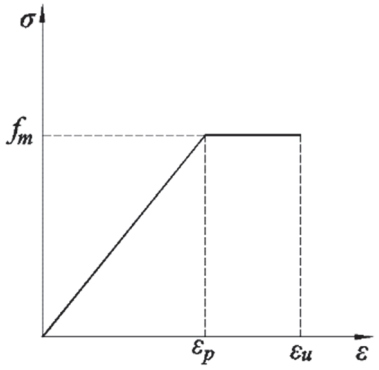

Figure 2 Compressive stress-strain curve of masonry

Note that the stress and strain of the section are positive with pressure, and the strain and stress of the section at the bottom of the wall are ε_c and σ_c respectively on the side with larger compressive strain, and ε_c' and σ_c' on the other side. With the increase of horizontal displacement, the failure process of the bottom and top sections of the wall is divided into three stages: elastic stage, elastoplastic stage and collapse stage.

3 LOAD-DISPLACEMENT CHARACTERISTICS OF WALL AT ELASTIC STAGE

When the horizontal load is small, the component is in the elastic stage. According to the structural stability theory, the relationship between the wall top displacement δ and the horizontal load P is obtained:

$$\Delta = \frac{PH^3}{12EI}\frac{1}{1-\frac{N}{N_e}} \tag{1}$$

In the formula, N_e is the critical load for the instability of the wall under axial compression.

$N_e = \frac{0.822N}{k\beta^2\varepsilon_p}$, $\frac{N}{N_e} = 1.216\varepsilon_p k\beta^2$, β is the wall height thickness ratio.

$\beta = \frac{H}{h}$, k is axial compression ratio.

$k = \frac{N}{f_m bh}$, $f_m = E\varepsilon_p$, h is for wall thickness; b is for wall width.

The following Eq. (2) can be deduced from Eq. (1).

$$\frac{P}{f_m bh} = \frac{1-1.216\varepsilon_p k\beta^2}{\varepsilon_p \beta^2}\frac{\Delta}{H} \tag{2}$$

Obviously, when Eq. (3) is satisfied, the wall will be unstable failure. On the contrary, the structure will be material failure. Before material failure, the bending moment at the bottom and top of the wall is shown in Eq. (4).

$$k \le \frac{1}{1.216\varepsilon_p \beta^2} \tag{3}$$

$$M = \frac{1-0.216\varepsilon_p k\beta^2}{1-1.216\varepsilon_p k\beta^2}\frac{PH}{2} \tag{4}$$

4 LOAD-DISPLACEMENT CHARACTERISTICS OF WALL IN ELASTOPLASTIC STAGE

4.1 Failure Pattern

When material failure occurs in the structure, the failure will occur at the bottom and top section of the wall with the maximum bending moment. According to the section, there are two kinds of failure modes: tensile damage and compression failure.

(1) When k is small, horizontal cracking occurs first on the side with small compressive strain, and then the side with large compressive strain changes to reach the ultimate

compressive strain ε_u. The structure is damaged in tension, as shown in Fig. 3.

(2) When k is larger, the peak compressive strain of masonry is ε_p on the side with larger compressive strain. Then horizontal cracking occurs on the side with low compressive strain. On the side with larger compressive strain, the ultimate compressive strain of masonry is ε_u. The structure is damaged under compression, as shown in Fig. 4.

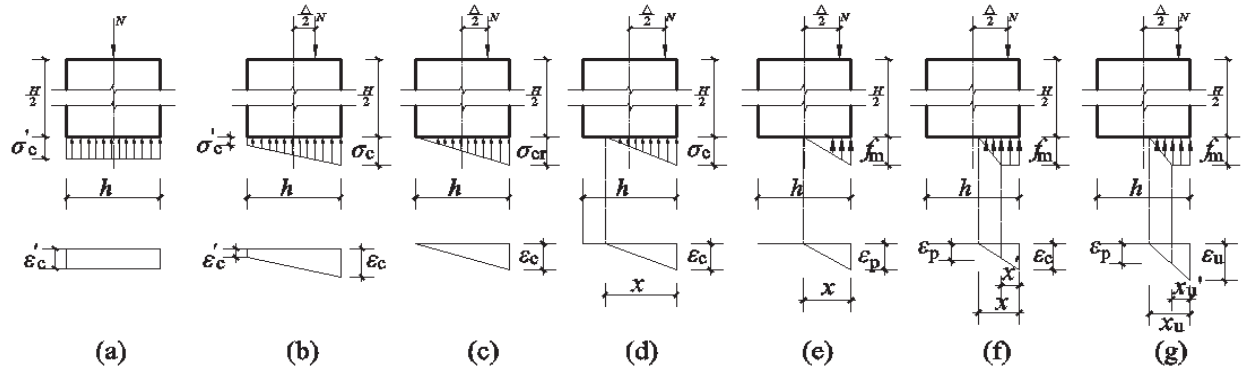

Figure 3 Tensile failure process and stress strain distribution of wall bottom section

Note: (a) Apply vertical load; (b) Elastic stage; (c) Will not crack (at the end of elastic stage); (d) Cracked, but the compression area remains elastic; (e) The maximum compressive strain reaches ε_p; (f) Cracking, elasto-plastic in compression zone; (g) Limit state, maximum compressive strain reaches ε_u

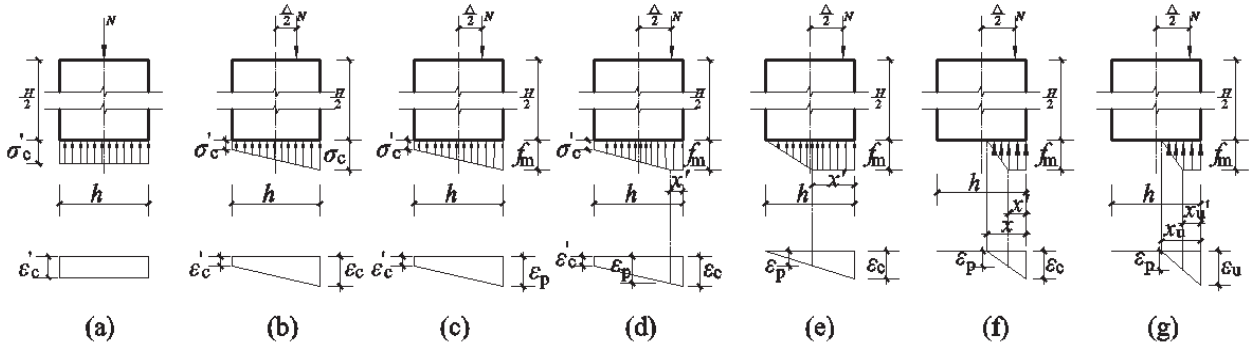

Figure 4 Compression failure process and stress strain distribution of wall bottom section

Note: (a) Apply vertical load; (b) Elastic stage; (c) The maximum compressive strain reaches ε_p (end of elastic stage); (d) Elastoplasticity in compression zone; (e) Will not crack; (f) Cracking, elasto-plastic in compression zone; (g) Limit state, maximum compressive strain reaches ε_u

When the maximum compressive strain of the section reaches the ultimate compressive strain, both kinds of failure rotate according to the resultant point of the rigid body around the compression zone of the section. Finally, the moment generated by the load reaches the resistance moment of the section and the wall collapses.

4.2 Tensile Damage

(1) Load (cracking) and displacement at the end of elastic stage

Ignoring the tensile strength of masonry, when cracking, $\sigma'_c = 0$, the horizontal cracking load is Eq. (5) and the cracking displacement is Eq. (6).

$$\frac{P_{cr}}{f_m bh} = \frac{(1-1.216\varepsilon_p k\beta^2)k}{3\beta(1-0.216\varepsilon_p k\beta^2)} \tag{5}$$

$$\frac{\Delta_{cr}}{H} = \frac{\varepsilon_p k\beta}{3-0.648\varepsilon_p k\beta^2} \tag{6}$$

As shown in Fig. 3c, the maximum compressive stress at the bottom of the wall at the time of cracking is σ_{cr} by taking an equilibrium in the y direction.

$$\sigma_{cr} = 2kf_m \tag{7}$$

Based on the assumption of flat section, the curvature of the wall bottom section is ϕ_{cr}.

$$\phi_{cr} = \frac{2k\varepsilon_p}{h} \tag{8}$$

(2) P-Δ curves after cracking ($\varepsilon_c < \varepsilon_p$)

With the increase of horizontal displacement, the bottom section of the cracked wall is detached, and the actual compression zone height of masonry is x. When $\varepsilon_c < \varepsilon_p$, the sectional stress presents a triangular distribution, and the maximum compressive stress $\sigma_c < f_m$, as shown in Fig. 3d.

Based on the equilibrium condition and the assumption of plane section, the curvature ϕ of section is obtained.

$$\phi = \frac{h^2}{x^2}\phi_{\mathrm{cr}} \tag{9}$$

More conservatively, it is considered that the displacement of the top of the wall is proportional to the

curvature, then the displacement of the top of the wall is obtained.

$$\Delta \simeq \left(\frac{h}{x}\right)^2 \cdot \Delta_{cr} \tag{10}$$

According to Eq. (10) and torque equilibrium condition, it can be obtained.

$$\frac{P}{f_m bh} = \frac{k}{\beta}\left(1 - \frac{2}{3}\sqrt{\frac{\Delta_{cr}}{\Delta}} - \frac{\Delta}{h}\right) \tag{11}$$

(3) Horizontal load and displacement when $\varepsilon_c = \varepsilon_p$

When $\varepsilon_c = \varepsilon_p$, the stress-strain of the wall bottom section is shown in Fig. 3e. Based on the assumption of plane section and equilibrium condition, the horizontal load P_p and the horizontal displacement Δp are obtained.

$$\frac{P_p}{f_m bh} = \frac{k}{\beta}\left(1 - \frac{4k}{3} - \frac{\Delta_{cr}}{4k^2 h}\right) \tag{12}$$

$$\Delta_p = \frac{\Delta_{cr}}{4k^2} \tag{13}$$

(4) P-Δ curves after cracking ($\varepsilon_p < \varepsilon_c < \varepsilon_u$)

When $\varepsilon_p < \varepsilon_c < \varepsilon_u$, the distribution of stress and strain at the section is shown in Fig. 3f. Based on the balance equation, physical equation, assumption of plane section and assumption that the displacement of wall top is proportional to the curvature, the following formula is obtained.

$$\frac{P}{f_m bh} = \frac{k}{\beta}\left[1 - \frac{\Delta}{h} - k - \frac{1}{48k^3}\left(\frac{\Delta_{cr}}{\Delta}\right)^2\right] \tag{14}$$

(5) Ultimate load and ultimate displacement

When $\varepsilon_c = \varepsilon_u$, the masonry on the compressive side is crushed, and the distribution of stress and strain on the section is shown in Fig. 3g. The ultimate displacement Δ_u and ultimate load P_u are obtained from the assumption of plane section and equilibrium condition.

$$\frac{\Delta_u}{H} = \frac{\left(\varepsilon_u - 0.5\varepsilon_p\right)\beta}{6k\left(1 - 0.216\varepsilon_p k\beta^2\right)} \tag{15}$$

$$\frac{P_u}{f_m bh} = \frac{k}{\beta}\left[1 - \frac{\Delta_u}{h} - k - \frac{1}{48k^3}\left(\frac{\Delta_{cr}}{\Delta_u}\right)^2\right] \tag{16}$$

4.3 Compression Failure

(1) The end of the elastic stage

When $\varepsilon_c = \varepsilon_p$, the stress-strain distribution of the section is shown in Fig. 4c. Based on the mechanics of materials and Eqs. (2) and (4), the horizontal load P_{p2} and the horizontal displacement Δ_{p2} at the end of the elastic stage are obtained.

$$\frac{P_{p2}}{f_m bh} = \frac{\left(1 - 1.216\varepsilon_p k\beta^2\right)\left(1 - k\right)}{3\beta\left(1 - 0.216\varepsilon_p k\beta^2\right)} \tag{17}$$

$$\frac{\Delta_{p2}}{H} = \frac{\left(1 - k\right)\varepsilon_p \beta}{3 - 0.647\varepsilon_p \beta^2 k} \tag{18}$$

The curvature of the wall bottom section is obtained.

$$\phi_{p2} = \frac{2\varepsilon_p}{h}(1 - k) \tag{19}$$

(2) Before cracking ($\varepsilon_p < \varepsilon_c < \varepsilon_u$) P-Δ curve

When $\varepsilon_p < \varepsilon_c < \varepsilon_u$, the stress-strain of the section is shown in Fig. 3d. Based on the balance equation, physical equation, assumption of plane section and assumption that the displacement of wall top is proportional to the curvature, the following formula is obtained.

$$\frac{P}{f_m bh} = \frac{k}{\beta}\left[\frac{1 - k}{k}\left(1 - \frac{2}{3}\sqrt{\frac{\Delta_{p2}}{\Delta}}\right) - \frac{\Delta}{h}\right] \tag{20}$$

(3) Cracking load and cracking displacement

With the increase of horizontal displacement, ε'_c decreases until $\varepsilon'_c = 0$, at which time the wall is in the state of uncracked, as shown in Fig. 4e. The corresponding horizontal displacement Δ_{cr2} and horizontal force P_{cr2} can be obtained according to the conditions of plane section and equilibrium.

$$\frac{\Delta_{cr2}}{H} = \frac{\beta\varepsilon_p}{4\left(1 - k\right)\left(3 - 0.6476\varepsilon_p \beta^2 k\right)} \tag{21}$$

$$\frac{P_{cr2}}{f_m bh} = \frac{k}{\beta}\left[\frac{1}{3k}\left(1 - k\right)\left(4k - 1\right) - \frac{1}{4\left(1 - k\right)^2}\frac{\Delta_{p2}}{h}\right] \tag{22}$$

(4) P-Δ curves after cracking ($\varepsilon_p < \varepsilon_c < \varepsilon_u$)

When $\varepsilon_p < \varepsilon_c < \varepsilon_u$, the section is cracked, and the stress-strain distribution is shown in Fig. 4f. According to the condition of plane section, physical equation, equilibrium condition and assumption that the displacement of wall top is proportional to the curvature, the following formula is obtained.

$$\frac{P}{f_m bh} = \frac{k}{\beta}\left[1 - k - \frac{1}{48k(1 - k)^2}\left(\frac{\Delta_{p2}}{\Delta}\right)^2 - \frac{\Delta}{h}\right] \tag{23}$$

(5) Ultimate load and ultimate displacement

When $\varepsilon_c = \varepsilon_u$, the stress-strain distribution of the section is shown in Fig. 4g. According to the assumption of plane section and equilibrium condition, the ultimate displacement Δ_{u2} and ultimate load P_{u2} are obtained.

$$\frac{\Delta_{u2}}{H} = \frac{\left(\varepsilon_u - 0.5\varepsilon_p\right)\beta}{6k\left(1 - 0.216\varepsilon_p \beta^2 k\right)} \tag{24}$$

$$\frac{P_{u2}}{f_m bh} = \\ = \frac{k}{\beta}\left[1-k-\frac{k}{12}\left(\frac{\varepsilon_p}{\varepsilon_u-0.5\varepsilon_p}\right)^2-\frac{\left(\varepsilon_u-0.5\varepsilon_p\right)\beta^2}{6k\left(1-0.216\varepsilon_p\beta^2 k\right)}\right] \quad (25)$$

5 LOAD-DISPLACEMENT CHARACTERISTICS OF WALL COLLAPSE STAGE

5.1 P-Δ curve before Collapse

When $\varepsilon_c > \varepsilon_u$, the wall approximately behaves as a rigid body rotating around the compression zone, and the stress and height of the compression zone remain unchanged. According to the equilibrium condition, the P-Δ relation of the wall is obtained.

$$\frac{P}{f_m bh} = \frac{k}{\beta}\left[1-\beta\frac{\Delta}{H}-\frac{1-\xi+0.33\xi^2}{1-\xi+0.25\xi^2}k\right] \quad (26)$$

In formula, $\xi = \varepsilon_p/\varepsilon_u$.

5.2 Case of Collapse

When the horizontal force $P = 0$ in the collapse stage, the wall collapses, and the unstable displacement of the wall is Δ_{ins}.

$$\frac{\Delta_{ins}}{H} = \frac{1}{\beta}\left(1-\frac{1-\xi+0.33\xi^2}{1-\xi+0.25\xi^2}k\right) \quad (27)$$

6 DISCUSSION

6.1 The Boundary between the Two Types of Damage

The boundary failure characteristics of tensile failure and compression failure are as follows. When the minimum compressive strain of section in elastic stage is 0, the maximum compressive strain of section reaches the peak compressive strain at the same time, namely $P_{cr} = P_{p2}$. According to Eqs. (5) and (17), the boundary axial compression ratio of the first and second types of failure is $k_1 = 0.5$.

6.2 P-Δ Curve of the Wall

(1) Tensile failure

According to Eqs. (2), (11), (14) and (26), dimensionless load-displacement curves $\frac{P}{f_m bh}-\frac{\Delta}{H}$ of tensile failure members with different coaxial pressure ratios can be drawn when $\beta = 18$, as shown in Fig. 5.

When $k < k_{1a}$, the wall collapses before the maximum compressive strain reaches ε_p. When $k_{1a} < k < k_{1b}$, the wall collapses before the maximum compressive strain of the section reaches ε_u. Two boundary values k_{1a} and k_{1b} are deduced according to the following equation and definition.

$$1-\frac{4k_{1a}}{3}-\frac{\varepsilon_p\beta^2}{4k_{1a}\left(3-0.648\varepsilon_p\beta^2 k_{1a}\right)} = 0 \quad (28)$$

$$1-k_{1b}-\frac{\left(2\varepsilon_u-\varepsilon_p\right)\beta^2}{4k_{1b}\left(3-0.648\varepsilon_p\beta^2 k_{1b}\right)}-\left(\frac{\varepsilon_p}{2\varepsilon_u-\varepsilon_p}\right)^2\frac{k_{1b}}{3} = 0 \quad (29)$$

When $\beta = 18$, $k_{1a} = 0.059$, $k_{1b} = 0.168$.

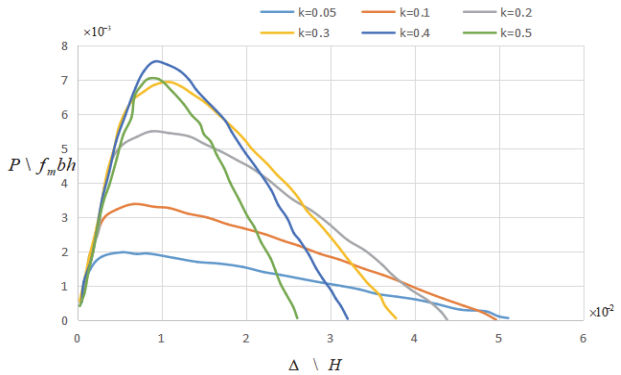

Figure 5 Load-displacement curve of tensile wall when $\beta = 18$

(2) Compression failure

According to Eqs. (2), (20), (23) and (26), the dimensionless load-displacement curve $\frac{P}{f_m bh}-\frac{\Delta}{H}$ of tensile failure members with different coaxial pressure ratios can be drawn when $\beta = 18$, as shown in Fig. 6.

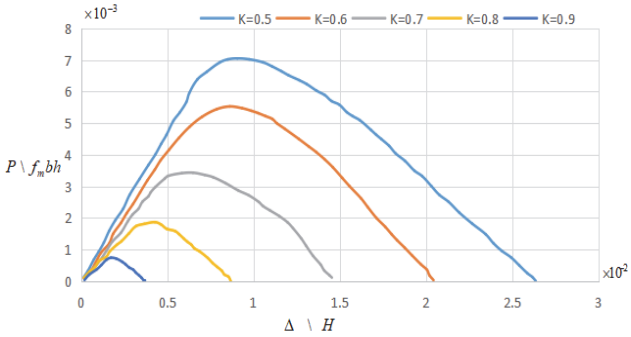

Figure 6 The load-displacement curve of the wall when $\beta = 18$

When $k_{2a} < k < k_{2b}$, the side with small compressive stress of section has cracked, but the maximum compressive strain of section does not reach ε_u, and the wall collapses. When $k_{2b} < k < 1$, the wall collapses before the maximum compressive strain of the section reaches ε_u, and the minimum compressive stress of the section is greater than 0 (full section compression). Two bound values k_{2a} and k_{2b} are derived from the definition and the equation below.

$$\xi^2\left[1-k_{2a}\xi-\sqrt{\xi(1-k_{2a})\left(2-\xi-k_{2a}\xi\right)}\right] \\ -2\left(1-k_{2a}\right)\left(1-\xi\right)^2 = 0 \quad (30)$$

$$\left(1-k_{2b}\right)\left(1-\frac{2}{3}\sqrt{\frac{1}{\gamma}}\right)-k_{2b}\gamma\beta\frac{\Delta_{p2}}{H} = 0 \quad (31)$$

In formula, $\gamma = \dfrac{\left(1-\xi\right)^2}{\left(1-k_{2b}\right)\xi^2+\xi\sqrt{\left(1-k_{2b}\xi\right)^2-\left(1-\xi\right)^2}}$

When $\beta = 18$, $k_{2a} = 0.777$, $k_{2b} = 0.975$.

6.3 Influence of Axial Compression Ratio and Height-Thickness Ratio on Horizontal Load and Displacement at the End of Elastic Stage

According to Eqs. (5) and (17) and (6) and (18), the variation rules of horizontal load, displacement and axial compression ratio at the end of elastic stage of walls with different height and thickness ratios can be obtained, as shown in Figs. 7 and 8.

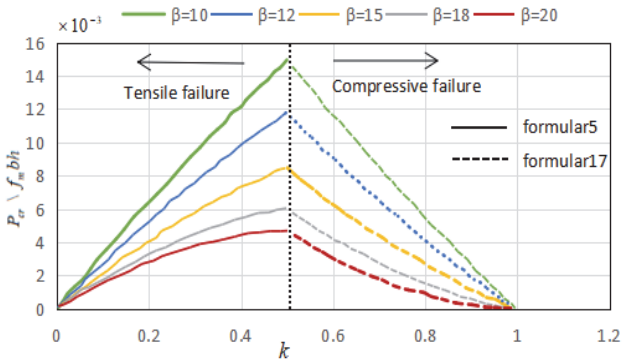

Figure 7 The relation between horizontal load and axial compression ratio and height-thickness ratio at the end of elastic stage

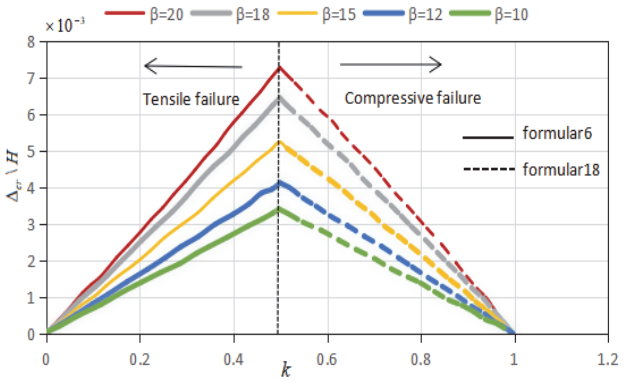

Figure 8 The relation between the displacement ratio and axial compression ratio and the ratio of height and thickness at the end of elastic stage

As can be seen from the figure, when tensile failure occurs, the horizontal load and interlayer displacement ratio at the end of the elastic stage increase with the axial compression ratio. As can be seen from the figure, in tensile failure, the horizontal load and interlayer displacement ratio at the end of the elastic stage increase with the increase of axial compression ratio, while the compression failure is on the contrary. The higher the ratio of height to thickness, the smaller the horizontal load at the end of the elastic stage and the larger the displacement ratio between horizontal layers.

6.4 Influence of Axial Compression Ratio and Height-Thickness Ratio on Ultimate Load and Ultimate Displacement

According to Eqs. (16) and (25), as well as Eqs. (15) and (24), the variation rules of ultimate load, ultimate displacement and axial compression ratio of walls with different height and thickness ratios can be obtained. As shown in Figs. 9 and 10, the following conclusions can be drawn from the figures.

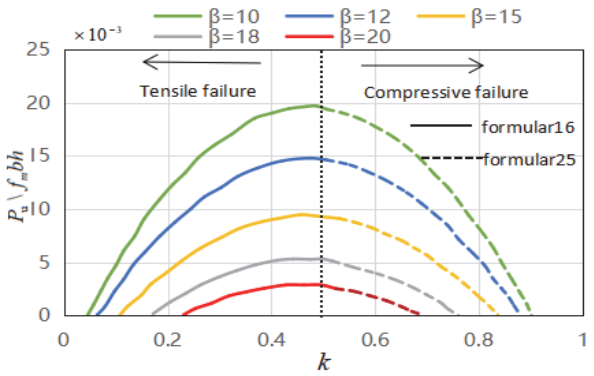

Figure 9 Variation law of wall ultimate load with axial compression ratio and height-thickness ratio

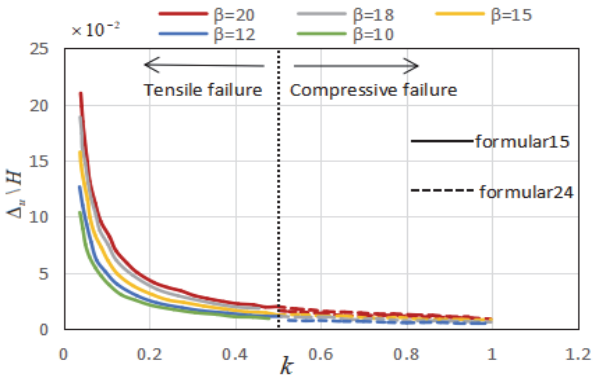

Figure 10 Variation law of ultimate interlayer displacement ratio of wall with axial compression ratio and height-thickness ratio

(1) The horizontal ultimate load of tensile failure increases with the increase of axial compression ratio, but the opposite is true of compressive failure.

(2) The horizontal ultimate load decreases with the increase of height-thickness ratio.

(3) When k is very small or very large (see 5.2 in this article), the wall collapse occurs when the maximum compressive strain does not reach ε_u, and the horizontal ultimate load is very small and can be ignored.

(4) The horizontal ultimate displacement ratio decreases with the increase of axial compression ratio, especially when the axial compression ratio $k < 0.2$, the ultimate displacement decreases sharply.

(5) The horizontal limit interlayer displacement ratio increases with the increase of height-thickness ratio.

6.5 Influence of Axial Compression Ratio and Height-Thickness Ratio on Collapse Displacement

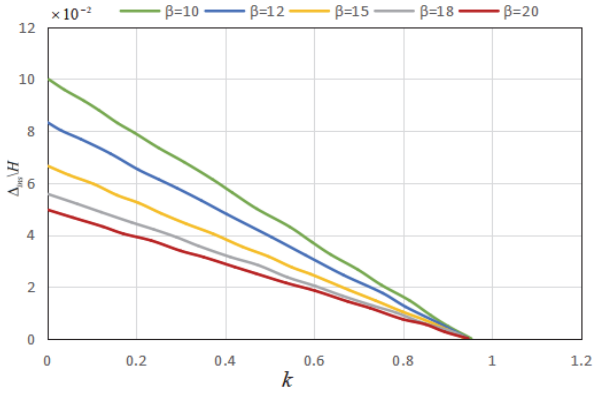

Figure 11 Variation law of unstable displacement with axial compression ratio and height-thickness ratio of wall collapse

According to Eq. (26), the variation law of unstable displacement with axial compression ratio during wall collapse can be obtained (Fig. 10). Fig. 11 shows that the inter-story displacement ratio decreases with the increase of axial compression ratio and height-thickness ratio. It is noted that when the axial compression ratio is very small, the wall collapse occurs when the maximum compressive strain does not reach ε_u, and the collapse displacement is not much different from that obtained by Eq. (26). When the axial compression ratio is very large, it is assumed that the stress distribution of the section at the collapse stage is the same as that under the ultimate load, and there is some error with the actual situation. However, the displacement ratio between collapsed layers is already very small, so it is 0 approximately, which is safe.

7 CONCLUSION

Based on basic assumptions, load displacement characteristics of unreinforced masonry bearing walls under out-of-plane loads are analyzed, and the following conclusions are obtained.

(1) The failure characteristics of unreinforced masonry walls under external load can be divided into tensile failure and compression failure.

(2) In tensile failure, the horizontal load and interlayer displacement ratio at the end of elastic stage increase with the increase of axial compression ratio, but the compression failure is the opposite. The higher the ratio of height to thickness, the smaller the horizontal load at the end of elastic stage and the larger the displacement ratio between horizontal layers.

(3) The horizontal ultimate load of tensile failure increases with the increase of axial pressure, but the opposite is true of compressive failure.

(4) The horizontal ultimate load of tensile failure increases with the increase of axial compression ratio, while the compressive failure is opposite. The horizontal ultimate load decreases with the increase of height-thickness ratio.

(5) The horizontal limit interlayer displacement ratio decreases with the increase of axial compression ratio and increases with the increase of height-thickness ratio.

(6) The displacement ratio between layers decreases with the increase of axial compression ratio and height-thickness ratio.

This article proposes a static elastic-plastic analysis method for unreinforced masonry structures based on the out of plane load position relationship of wall panels, which provides a better development for the design method of unreinforced masonry structures.

8 REFERENCE

[1] Wang, C. (2010). Investigation and analysis of building structure damage in Yushu Earthquake. *Building structure*, *40*(8), 106-109.

[2] Ferreira, T. M., Costa, A. A., & Costa, A. (2015). Analysis of the out-of-plane seismic behavior of unreinforced masonry: A literature review. *International Journal of Architectural Heritage*, *9*(8), 949-972. https://doi.org/10.1080/15583058.2014.885996

[3] Sharma, S., Grottoli, L., Tomassetti, U., & Graziotti, F. (2020). Dataset from shake-table testing of four full-scale URM walls in a two-way bending configuration subjected to combined out-of-plane horizontal and vertical excitation. *Data in Brief*, *31*, 105851. https://doi.org/10.1016/j.dib.2020.105851

[4] Jiang, L., Jiang, L., Li, X., Zhang, F., & Zheng, S., (2021). Shaking table test and seismic performance assessment of unreinforced multi-storey masonry residence. *Journal of Building Structures*, *42*(8), 25-35. https://doi.org/10.14006/j.jzjgxb.2019.0144

[5] Deng, M. K., Donf, Z. F., Yang, S., Wang, L., & Zhou, T. G. (2019). Shaking table test on damaged masonry structure reinforced with high ductile concrete layer. *Engineering Mechanics*, *36*(7), 116-125. https://doi.org/10.6052/j.issn.1000-4750.2018.03.0185

[6] Zhang, L. M., Wang, X. S., Cong, Y., Wang, Z. Q., & Liu, J. (2023). Transfer mechanism and criteria for static-dynamic failure of granite under true triaxial unloading test. *Geomechanics and Geophysics for Geo-Energy and Geo-Resources*, *9*, 104. https://doi.org/10.1007/s40948-023-00645-w

[7] Hussein, M. N., Alkadhimi, A., Najim, W. A., &Almousawi, H. A. (2021). Shaking table experiment on seismic performance of a scaled-down arch dam with initial crack. *International Journal of Design & Nature and Ecodynamics*, *16*(6), 683-689. https://doi.org/10.18280/ijdne.160610

[8] Li, J. L., Zhang, S. R., Wang, S. L., Liu, Z. H., & Hao, Y. Z. (2020). Shaking table tests on the seismic response of a columnless subway station with asymmetric load under bidirectional seismic action. *International Journal of Safety and Security Engineering*, *10*(4), 559-566. https://doi.org/10.18280/ijsse.100416

[9] Wang, P. S., Ding, H. Y., & Zhang, P. Y. (2020). Shaking table tests and numerical analysis on the seismic response of karst-crossing socketed piles in dry sandy soil foundation. *International Journal of Design & Nature and Ecodynamics*, *15*(5), 701-709. https://doi.org/10.18280/ijdne.150512

[10] Muhit, I. B., Masia, M. J., Stewart, M. G., & Isfeld, A. C. (2022). Spatial variability and stochastic finite element model of unreinforced masonry veneer wall system under Out-of-plane loading. *Engineering Structures*, *267*, 114674. https://doi:10.1016/J.ENGSTRUCT.2022.114674

[11] Giresini, L., Fragiacomo, M., & Lourenço, P. B. (2015). Comparison between rocking analysis and kinematic analysis for the dynamic out-of-plane behavior of masonry walls. *Earthquake Engineering & Structural Dynamics*, *44*(13), 2359-2376. https://doi.org/10.1002/eqe.2592

[12] Jiang, L. X., Wang, Z. L., & Zhang, F. W. (2021). Displacement-based and ductility-based seismic performance assessment method of existing multi-story regular masonry structures. *Building Structure*, *42*(3), 72-79.

[13] Lagomarsino, S. (2015). Seismic assessment of rocking masonry structures. *Bulletin of Earthquake Engineering*, *13*, 97-128. https://doi.org/10.1007/s10518-014-9609-x

[14] Zhang, L., Chao, W., Liu, Z., Cong, Y., & Wang, Z. (2022). Crack propagation characteristics during progressive failure of circular tunnels and the early warning thereof based on multi-sensor data fusion. *Geomechanics and Geophysics for Geo-Energy and Geo-Resources*, *8*(5), 172. https://doi.org/10.1007/s40948-022-00482-3

[15] Bui, T. T., Limam, A., & Sarhosis, V. (2021). Failure analysis of masonry wall panels subjected to in-plane and out-of-plane loading using the discrete element method. European *Journal of Environmental and Civil Engineering*, *25*(5), 876-892. https://doi.org/10.1080/19648189.2018.1552897

[16] Chang, L. Z., Rots, J. G., & Esposito, R. (2021). Influence of aspect ratio and pre-compression on force capacity of unreinforced masonry walls in out-of-plane two-way bending. *Engineering Structures*, *249*, 113350. https://doi.org/10.1016/j.engstruct.2021.113350

[17] Jiang, Y. P., Su, L., & Huang, X. (2020). Seismic fragility analysis of unreinforced masonry structures considering

parameter uncertainties. *Engineering Mechanics*, *37*(1), 159-167. https://doi.org/10.6052/j.issn.1000-4750.2019.01.0068
[18] Zhang, L. M., Cong, Y., Meng, F. Z., Wang, Z. Q., Zhang, P., & Gao, S. (2021). Energy evolution analysis and failure criteria for rock under different stress paths. *Acta Geotechnica*, *16*(2), 569-580. https://doi.org/10.1007/s11440-020-01028-1
[19] Mauro, A., de Felice, G., & DeJong, M. J. (2015). The relative dynamic resilience of masonry collapse mechanisms. *Engineering Structures*, *85*, 182-194. https://doi.org/10.1016/j.engstruct.2014.11.021
[20] Bovo, M. & Buratti, N. (2019). Evaluation of the variability contribution due to epistemic uncertainty on constitutive models in the definition of fragility curves of RC frames. *Engineering Structures*, *188*, 700-716. https://doi.org/10.1016/j.engstruct.2019.03.064
[21] Zhang, L. M., Zhang, D., Cong, Y., Wang, Z. Q., & Wang, X. S. (2023). Constructing a three-dimensional creep model for rocks and soils based on memory-dependent derivatives: A theoretical and experimental study. *Computers and Geotechnics*, *159*, 105366. https://doi.org/10.1016/j.compgeo.2023.105366
[22] Quagliarini, E., Maracchini, G., & Clementi, F. (2017). Uses and limits of the Equivalent Frame Model on existing unreinforced masonry buildings for assessing their seismic risk: A review. *Journal of Building Engineering*, *10*, 166-182. https://doi.org/10.1016/j.jobe.2017.03.004
[23] Di Domenico, M., Ricci, P., & Verderame, G. M. (2020). Experimental assessment of the influence of boundary conditions on the out-of-plane response of unreinforced masonry infill walls. *Journal of Earthquake Engineering*, *24*(6), 881-919. https://doi:10.1080/13632469.2018.1453411
[24] Muhit, I. B., Masia, M. J., & Stewart, M. G. (2022). Monte-Carlo laboratory testing of unreinforced masonry veneer wall system under out-of-plane loading. *Construction and Building Materials*, *321*, 126334. https://doi.org/10.1016/j.conbuildmat.2022.126334

Contact information:

Liu SHI
(Corresponding author)
Hunan Trinity industrial Vocational and Technical College,
Changsha 410129, China
E-mail: 1248987991@qq; shil62@sany.com.cn

Jingyuan GUO
Hunan Trinity industrial Vocational and Technical College,
Changsha 410129, China
E-mail: guojy9@sany.com.cn

Songlin ZHAO
Hunan Chemical Engineering Design Institute Co. LTD,
Changsha 410000, China
E-mail: 15111119149@163.com

Jianguo LIANG
Hunan Trinity industrial Vocational and Technical College,
Changsha 410129, China
College of Civil Engineering, Changsha University of Science and Technology,
Changsha 410114, China
E-mail: liangjg9@sany.com.cn

Guanxing CHEN
Hunan Trinity industrial Vocational and Technical College,
Changsha 410129, China
E-mail: chengx44@sany.com.cn